Science of the Total Environment 625 (2018) 416–427

Contents lists available at ScienceDirect

Science of the Total Environment

journal homepage: www.elsevier.com/locate/scitotenv

Substantial impacts of landscape changes on summer climate with major regional differences: The case of China

Qian Cao [a], Deyong Yu [a,*], Matei Georgescu [b], Jianguo Wu [a,c,**]

[a] Center for Human-Environment System Sustainability (CHESS), State Key Laboratory of Earth Surface Processes and Resource Ecology (ESPRE), Faculty of Geographical Science, Beijing Normal University, Beijing 100875, China
[b] School of Geographical Sciences and Urban Planning, Urban Climate Research Center, Arizona State University, Tempe, AZ 85287, United States
[c] School of Life Sciences and School of Sustainability, Arizona State University, Tempe, AZ 85287, United States

HIGHLIGHTS

- Numerical simulations with incorporation of satellite-derived landscape patterns.
- Large-scale impacts of land cover and land management change on summer climate.
- Heterogeneous climatic effects in space with identified hotspots.

GRAPHICAL ABSTRACT

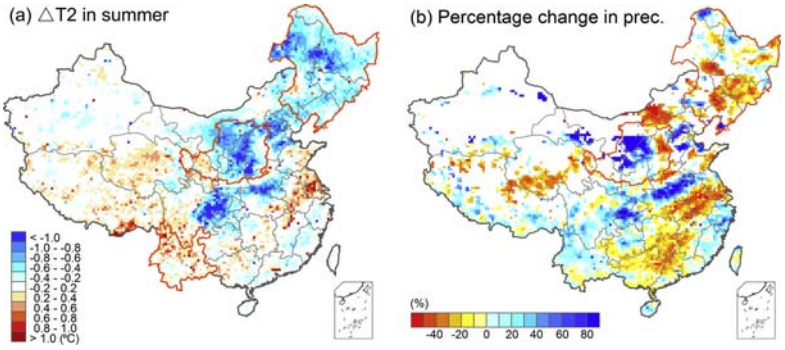

ARTICLE INFO

Article history:
Received 8 August 2017
Received in revised form 20 December 2017
Accepted 23 December 2017
Available online xxxx

Editor: R Ludwig

Keywords:
Land cover change
Land management change
Land surface biophysical property
Climate change
WRF

ABSTRACT

China's rapid socioeconomic development during the past few decades has resulted in large-scale landscape changes across the country. However, the impacts of these land surface modifications on climate are yet to be adequately understood. Using a coupled process-based land-atmospheric model, therefore, we quantified the climatic effects of land cover and land management changes over mainland China from 2001 to 2010, via incorporation of real-time and high-quality satellite-derived landscape representation (i.e., vegetation fraction, leaf area index, and albedo) into numerical modeling. Our results show that differences in landscape patterns due to changes in land cover and land management have exerted a strong influence on summer climate in China. During 2001 and 2010, extensive cooling of up to 1.5 °C was found in the Loess Plateau and 1.0 °C in northeastern China. In contrast, regional-scale warming was detected in the Tibetan Plateau (0.3 °C), Yunnan province (0.4 °C), and rapidly expanding urban centers across China (as high as 2 °C). Summer precipitation decreased in the northeastern region, with patchy reduction generally <1.8 mm/day, but increased in the Loess Plateau, with local spikes up to 2.4 mm/day. Our study highlights that human alterations of landscapes have had substantial impacts on summer climate over the entire mainland China, but these impacts varied greatly on the regional scale, including changes in opposite directions. Therefore, effective national-level policies and regional land management strategies for climate change mitigation and adaptation should take explicit account of the spatial heterogeneity of landscape-climate interactions.

* Correspondence to: D. Yu, No.19 XinJieKouWai Street, Beijing 100875, China.
** Correspondence to: J. Wu, P.O. Box 874501, Tempe, AZ 85287-4501, United States.
E-mail addresses: ydy@bnu.edu.cn (D. Yu), Jingle.Wu@asu.edu (J. Wu).

https://doi.org/10.1016/j.scitotenv.2017.12.290
0048-9697/

1. Introduction

Land use and land cover change have been a major driver of climate change at regional and global scales (Feddema et al., 2005; Foley et al., 2005; Kabat, 2004; Marland et al., 2003; NRC, 2005; Vitousek et al., 1997) because it affects the climate system through two general pathways: biogeochemical and biogeophysical (Feddema et al., 2005). Prior studies have demonstrated that biogeophysical effects resulting from modification of land surface properties can lead to regional climate change that is on the same order of magnitude as impacts owing to biogeochemical effects due to greenhouse gas emissions (Betts et al., 2007; Georgescu et al., 2013; Pielke and Avissar, 1990). This is because alterations to land surface biophysical properties modify surface energy budget and land-atmospheric transport of heat, moisture, and momentum, with additional consequences for temperature, air circulation, and precipitation change (Pielke et al., 2011, 2016). Therefore, accurately quantifying anthropogenic influence on climate requires consideration of biogeophysical processes (Davin et al., 2007; Mahmood et al., 2014, 2016; de Noblet-Ducoudré et al., 2012), particularly for regions experiencing dramatic land surface modification.

China has witnessed unprecedented socioeconomic transformations in recent decades and intensified human activities (e.g., urbanization, agricultural intensification, and reforestation) have dramatically modified ecosystems and landscapes across the nation (Liu et al., 2014). This has been especially evident since 2000, when urbanization entered a phase of rapid development (Wu et al., 2014) and implementation of the Grain to Green Program became prevalent nationwide (Feng et al., 2016; Gao et al., 2016). Increased utility of numerical modeling approaches to estimate climate effects of landscape changes for China as a whole improved our understanding of land-atmosphere interactions in this rapidly changing part of the planet (Fu, 2003; Hu et al., 2015; Wang et al., 2013; Wang et al., 2015; Xu et al., 2015). These studies focused mainly on comparing effects of potential natural vegetation with those of current land surface conditions. In contrast, few studies have examined the possible effects of historical landscape changes on regional climate in China. This was partly because climate effects spanning a time period of several decades may not be easily detected when only including changes in land cover classes.

However, land management change (LMC, e.g., the influence of different grazing intensities on grassland characteristics) can have similar or greater effects on land surface biophysical properties and therefore regional climate than land cover change (LCC, e.g., the conversion from forests to croplands). It is important to recognize that LMC may be independent of LCC. To date, limited research exists examining climate impacts of LMC that occurs within the same land cover type and does not result in LCC (Luyssaert et al., 2014). Although the representation of LMC has been restricted by inadequate data availability and excessive computing demands, omission of this subgrid-scale landscape heterogeneity will result in underestimation of climate effects and reduced skill of model performance (Cao et al., 2015; Georgescu et al., 2009; Pielke and Avissar, 1990; Weaver and Avissar, 2001). Fortunately, recent advances in remote sensing techniques and computational capacity facilitate the usage of real-time and high-quality data to characterize landscape changes induced by LCC and LMC.

Here we apply the Weather Research and Forecasting (WRF) Model (Skamarock and Klemp, 2008) to quantify impacts of landscape changes on summer climate over China. Our study focuses on summer season (we define summer as June, July, and August) because vegetation matures to peak greenness and thus exerts the strongest influence on land-atmosphere interactions during this period of time. We parameterized WRF on a 30-km basis using satellite-derived landscape patterns corresponding to 2001 and 2010, which differed in the representation of land cover and land surface biophysical properties (i.e., vegetation fraction, leaf area index, and surface albedo). We seek to answer the following questions: 1) Did land cover change or land management change result in greater landscape changes in China during 2001–2010? 2) Did these landscape changes have any major effects on regional climate across the country? 3) How did the climate effects of landscape changes vary spatially from region to region?

2. Materials and methods

2.1. Model configuration and parameterization

Simulations were performed using the Weather Research and Forecasting (WRF) model with the advanced dynamical core. The WRF model was configured with a one-way domain having grid spacing of 30 km in both horizontal directions (Fig. 1). The domain was centered on 36.5°N and 103°E with 200 grid cells along east-west direction and 170 grid cells along north-south direction, encompassing the entirety of China and portions of the Indian and Pacific Oceans, with a total area of 6000 × 5100 km^2. This domain configuration was deemed sufficiently expansive to capture the influence of the East Asian Monsoon on summer climate in China (Hu et al., 2015). A Lambert conformal conic projection was used for the model's horizontal coordinate while the model's vertical coordinate employed 30 terrain-following eta levels from the surface to 50 hPa. The initial and lateral boundary conditions for large-scale atmospheric fields were obtained from the Global Final Analysis (FNL) data archive, maintained by the National Centers for Environmental Prediction (NCEP; http://rda.ucar.edu/), with a 6-h temporal frequency and 1° grid spacing in both horizontal directions.

The main physical parameterizations used for all simulations are presented in Table 1. In order to represent land surface processes, the community Noah land surface model (LSM; Chen and Dudhia, 2001; Ek et al., 2003) coupled with the WRF model was utilized to simulate the energy and momentum exchange between the land surface and overlying atmosphere. However, although the coupled Noah LSM has been widely used to facilitate regional climate modeling, deficiencies exist with its prescribed land surface biophysical properties (Cao et al., 2015). In this work, therefore, we employed recently developed satellite-estimated landscape data with more detailed biogeographic information to improve characterization of landscape in the Noah LSM, and above all, to represent modification of biophysical properties arising from land management change.

2.2. Remotely sensed data acquisition

We obtained land cover data from the Data Center for Resources and Environmental Sciences, constructed by the Chinese Academy of Sciences (http://www.resdc.cn). The land cover data for 2000 and 2010 were derived from Landsat TM imagery with a spatial resolution of 1 km × 1 km. The data were classified according to the International

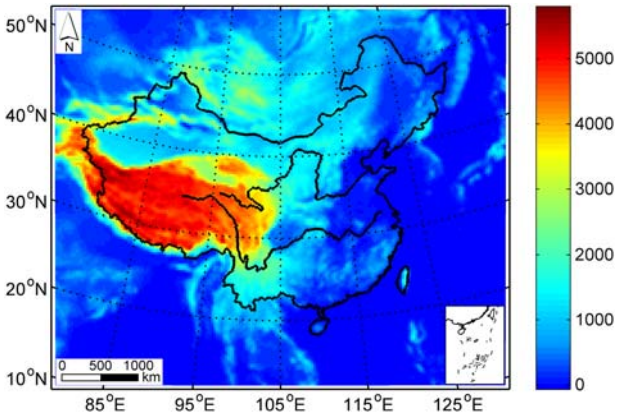

Fig. 1. Illustration of the model domain used in the WRF (Weather Research and Forecasting) simulations with topography overlaid (unit: m). The bottom-right rectangle illustrates the South China Sea Islands (the same below).

Table 1
Main physical parameterizations used for all simulations.

Model version	Version 3.6.1
Horizontal grid	ΔX and ΔY = 30 km
Number of points	200 (X direction), 170 (Y direction)
Vertical levels	30 levels
Time step	90 s
Radiation scheme	RRTM[a] (longwave); RRTMG[b] (shortwave)
Land surface model	Noah LSM
Cumulus scheme	K-F[c] (turned on)
Microphysics scheme	WSM-3[d]
PBL scheme	YSU[e]
Surface layer	MM5 similarity[f]
Initial and lateral boundary conditions	NCEP FNL

[a] RRTM, the Rapid Radiative Transfer Model.
[b] RRTMG, a new version of RRTM.
[c] K-F, the new Kain-Fritsch cumulus convective scheme.
[d] WSM-3, the WRF Single-Moment 3 class microphysics scheme.
[e] YSU, the Yonsei University planetary boundary layer (PBL) scheme.
[f] MM5 similarity, the revised MM5 Monin-Obukhov scheme.

Geosphere-Biosphere Program (IGBP) land use classification scheme, with an overall classification accuracy of 83.14% (Wu et al., 2013). The 1-km data were aggregated to the domain resolution by calculating the dominant land cover category in each 30-km grid cell. The newly developed data were then used within China, and for regions outside, the default IGBP-Modified MODIS 20-category land cover data, provided by the WRF modeling system, were employed.

We derived vegetation fraction from 1-km, 16-day MODIS vegetation indices data products (https://lpdaac.usgs.gov/), following the method below (Gutman and Ignatov, 1998):

$$\mathrm{FVC} = (N - N_s)/(N_v - N_s) \quad (1)$$

where FVC represents the fractional vegetation cover, N the NDVI at each pixel, N_s the bare soil NDVI, and N_v the dense vegetation NDVI. Here, the N_s and N_v were defined as the lower and upper 5% NDVI of the simulation domain, respectively (Sellers et al., 1996). Leaf area index (LAI) was provided by the global land surface satellite product (GLASS; http://glass-product.bnu.edu.cn/), with a spatial resolution of 0.05° × 0.05° for 46 retrieval periods per year (i.e., 1, 9,…, 361). Field validation has shown that the uncertainty of GLASS LAI was less than that of MODIS LAI (Xiao et al., 2014). Surface albedo was obtained from 30-arc, 8-day global gap-filled, snow-free albedo data archive (ftp://rsftp.eeos.umb.edu/). A temporal interpolation technique has been applied to the spatially complete albedo data set so as to fill the MODIS albedo product not having observations, being low quality, or being snow-covered with geophysical realistic values (Moody et al., 2008). The data set currently included white-sky and black-sky albedo, which are numerically related to each other as follows (Liang et al., 2005):

$$\alpha = f_{dir}\,\alpha_{dir} + f_{dif}\,\alpha_{dif} \quad (2)$$

$$f_{dir} + f_{dif} = 1 \quad (3)$$

where α denotes the blue-sky albedo, α_{dir} the black-sky albedo, and α_{dif} the white-sky albedo. f_{dir} and f_{dif} are proportions of direct beam and diffuse illumination in total incoming light. In this work, the f_{dif} was estimated as a function of solar zenith angle (Long and Gaustad, 2004). The 16-day and 8-day landscape data were then linearly interpolated to a daily interval and aggregated to the domain resolution (i.e., 30 km) via bilinear interpolation.

2.3. Numerical simulation design

We designed two numerical experiments to analyze impacts of landscape change on China's summer climate. One represented 2001 landscape (hereafter LS2001) by using 2000 land cover data (in lieu of 2001, which was unavailable) and 2001 biophysical properties (i.e., vegetation fraction, LAI, and surface albedo). The other denoted 2010 landscape (hereafter LS2010) by using 2010 land cover data and 2010 biophysical properties. To better distinguish the signal of landscape change-induced forcing, we selected a normal monsoon year as driving meteorology based on examination of the East Asian summer monsoon index (Li and Zeng, 2005). The year 2001 was chosen because the normalized value of the monsoon index was $<1\,\sigma$ in that year. Each experiment was then carried out with three independent realizations, initialized on January 1st, January 8th, and January 15th, 2001, respectively, and terminated on March 1st, 2002 (Table 2). Output before March 1st, 2001 was used as spin-up and therefore discarded.

When illustrating climate effects due to landscape changes, all three realizations for a particular experiment were averaged and subsequently differentiated. This ensemble approach is invaluable for the reduction of internal model noise and sensitivity to initial conditions, thus adding confidence to the simulation results (Georgescu et al., 2013). In addition, the pairwise comparison test (see supplementary information in Georgescu et al., 2013) was used to test the robustness of simulated 2-m air temperature and precipitation differences. If all three pairs of realizations (i.e., LS2010 – LS2001) in a grid cell will produce a trend of same signal (e.g., warming effects owing to landscape changes), we deem it robust impact. We further enhanced the criteria defined here by additionally requiring the absolute values of temperature and precipitation changes to exceed 0.2 °C and 0.6 mm/day, respectively.

2.4. Model evaluation data

Observations used for evaluating the spatially explicit model performance were obtained from the CN05.1 data set, provided by the National Climate Center of China (http://www.ncc-cma.net). This gridded data set was generated based on interpolation of 751 meteorological stations across mainland China for the purpose of climate model evaluation (Xu et al., 2009). The data set contains monthly climatological information (i.e., air temperature and precipitation) covering a period from 1961 to present, with a horizontal grid spacing of 0.25° in both directions. To facilitate model examination, mean summertime 2-m air temperature and precipitation, averaged across all three realizations from LS2001 and LS2010, respectively, were compared with the corresponding gridded observations from 2001.

In addition, we used the observation minus reanalysis (OMR; Kalnay and Cai, 2003) approach to evaluate 2-m air temperature differences due to landscape changes simulated by the WRF model. The data used for the OMR analysis included the NCEP-DOE (Department of Energy) reanalysis (Kanamitsu et al., 2002) and station-based observations provided by the China Meteorological Data Service Center (Xu et al., 2009; http://data.cma.cn/). Prior to applying the OMR analysis, the station-based observations were homogenized using the method proposed by Li and Yan (2009). Temperature trends in summer for a time series of 13 years (from 1999 to 2011) were calculated at each station in the

Table 2
Description of all simulations performed. LS2001: simulations using 2000 land cover data and 2001 land surface biophysical properties (i.e., vegetation fraction, leaf area index, and surface albedo). LS2010: simulations using 2010 land cover data and land surface biophysical properties.

Simulations	Spin-up period	Analysis time
LS2001	Jan 01 – Feb 28, 2001	Mar 01, 2001 – Mar 01, 2002
	Jan 08 – Feb 28, 2001	Mar 01, 2001 – Mar 01, 2002
	Jan 15 – Feb 28, 2001	Mar 01, 2001 – Mar 01, 2002
LS2010	Jan 01 – Feb 28, 2001	Mar 01, 2001 – Mar 01, 2002
	Jan 08 – Feb 28, 2001	Mar 01, 2001 – Mar 01, 2002
	Jan 15 – Feb 28, 2001	Mar 01, 2001 – Mar 01, 2002

identified hotspots using the station-based observations and gridded reanalysis data, respectively. The differences in the trends of 2-m air temperature variations between those derived from the observations and those derived from the reanalysis can then be used to evaluate landscape change-induced temperature changes.

3. Results

3.1. WRF model evaluation

Prior to examining model sensitivity to landscape changes, simulations from LS2001 and LS2010 were evaluated against gridded observations from 2001, respectively, to gauge the skill of model performance. Results show that the WRF model correctly represented the spatial variability of gridded observations in mainland China (Fig. 2). In summer, the model captured the observed temperature variability fairly well, with high temperatures simulated in eastern China and the Tarim Basin in northwestern China, as well as low temperatures in the Tibetan Plateau and the north of the Tarim Basin. The spatial correlation coefficient between the observation and simulation from LS2001 was 0.91. Also, the model properly reproduced the observed summer precipitation with reasonable fidelity, with low precipitation in the north of the Yangtze River and high precipitation to the south, with a spatial correlation coefficient equal to 0.73. However, a greater precipitation amount appeared along the border of southwestern China. This was mainly due to the intrinsic limitation of WRF-simulated precipitation at high elevation. Overall, the spatial variability of simulated 2-m air temperature and precipitation show reasonable agreement with the gridded observations, thus providing confidence in the model's capability to accurately capture the climatological behavior of mainland China during the simulated time period.

3.2. Landscape changes in China from 2001 to 2010

We first demonstrate that landscape changes over China during the previous decade was mainly attributed to LMC rather than LCC. From 2000 to 2010, the general pattern of land cover types in China underwent changed in two major ways (Fig. 3). First, extensive areas of cultivated fields and overgrazed lands (135,000 km^2) were converted to woodlands in the central part of the nation due to the Grain to Green Program. Second, scattered regions of croplands (36,000 km^2) in the eastern portion of China were lost owing to urban expansion. Meanwhile, forest areas increased (by 16,000 km^2) while barren lands were reduced somewhat (by 5000 km^2). It is worth noting that except urban expansion (which underwent rapid development throughout the period), changes in class areas did not occur at an equal rate over the decade. Instead, land cover transformation in China mainly took place after 2005.

Compared with LCC, changes in land surface biophysical properties due to LMC were considerably more extensive (Figs. 4a–c). In summer, vegetation fraction increased in northern China but decreased in southern portions, especially in the southwest. LAI increased in most areas, although patchy decreases were still found in southwestern and eastern portions of China. Unlike changes in vegetation fraction, surface albedo decreased in northern portions while increasing over southern portions of the country. Notably, alterations to biophysical characteristics were most apparent in the Loess Plateau (the region marked with a black solid contour), where vegetation fraction increased by 8–17%, LAI by 0.2–0.6, while surface albedo was reduced by 0.03–0.045 (Fig. 4d). In fact, the mean summertime NDVI and LAI progressively increased from 2000 to 2010 ($p < 0.01$), while the temporal evolution of surface albedo exhibited the opposite trend ($p < 0.05$; see insets in Fig. 4d).

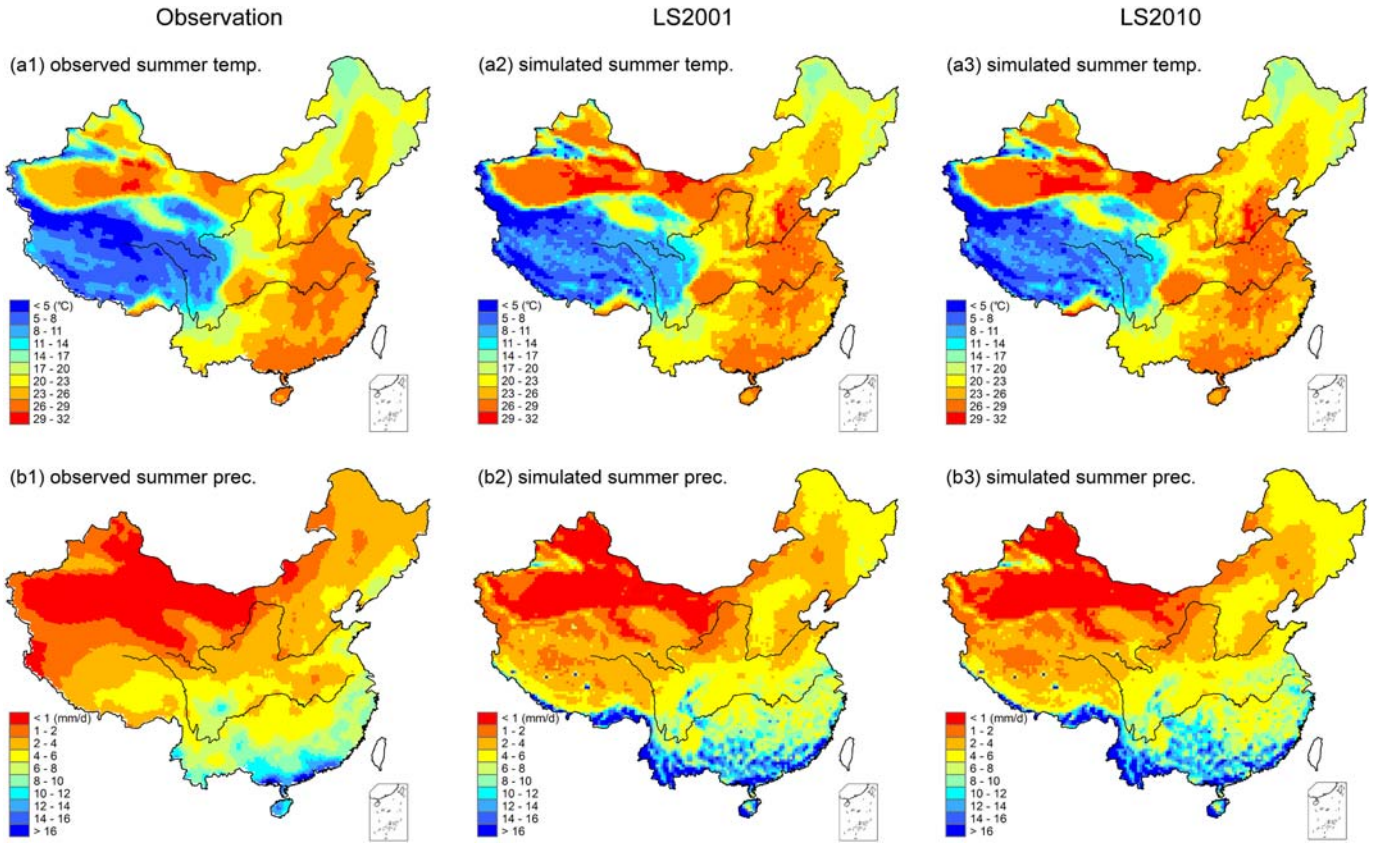

Fig. 2. Observed summertime 2-m air temperature (unit: °C) and precipitation (unit: mm/day) from 2001 (a1 and b1), simulated summertime 2-m air temperature and precipitation from LS2001 (a2 and b2), and simulated summertime 2-m air temperature and precipitation from LS2010 (a3 and b3).

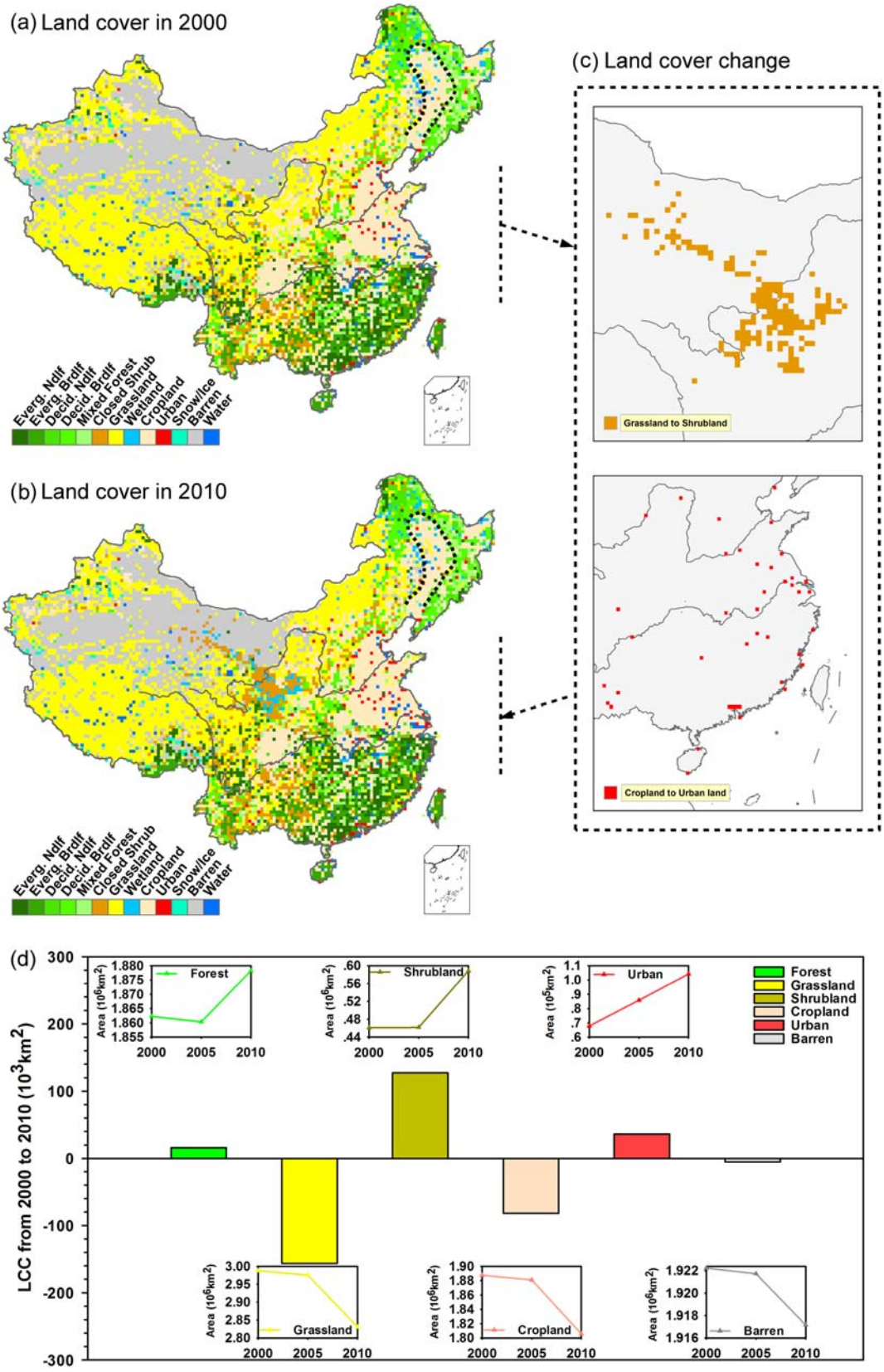

Fig. 3. Spatial pattern of land cover in 2000 (a), spatial pattern of land cover in 2010 (b), major land cover change between 2000 and 2010 (c), and areas of land cover change (LCC; unit: 10^3km^2) between 2000 and 2010 (d). The insets in (d) illustrate the temporal evolution of class areas. The farm belt in the Northeast of China is marked with a black dashed contour.

Consistent with statistically significant changes documented for the Loess Plateau, we also find that in contrast with its surroundings, both vegetation fraction and LAI increased conspicuously while surface albedo decreasing in the farm belt of the Northeast (the region marked with a black dashed contour in Fig. 3). Conversely, maximum decreases in vegetation fraction and LAI with widespread

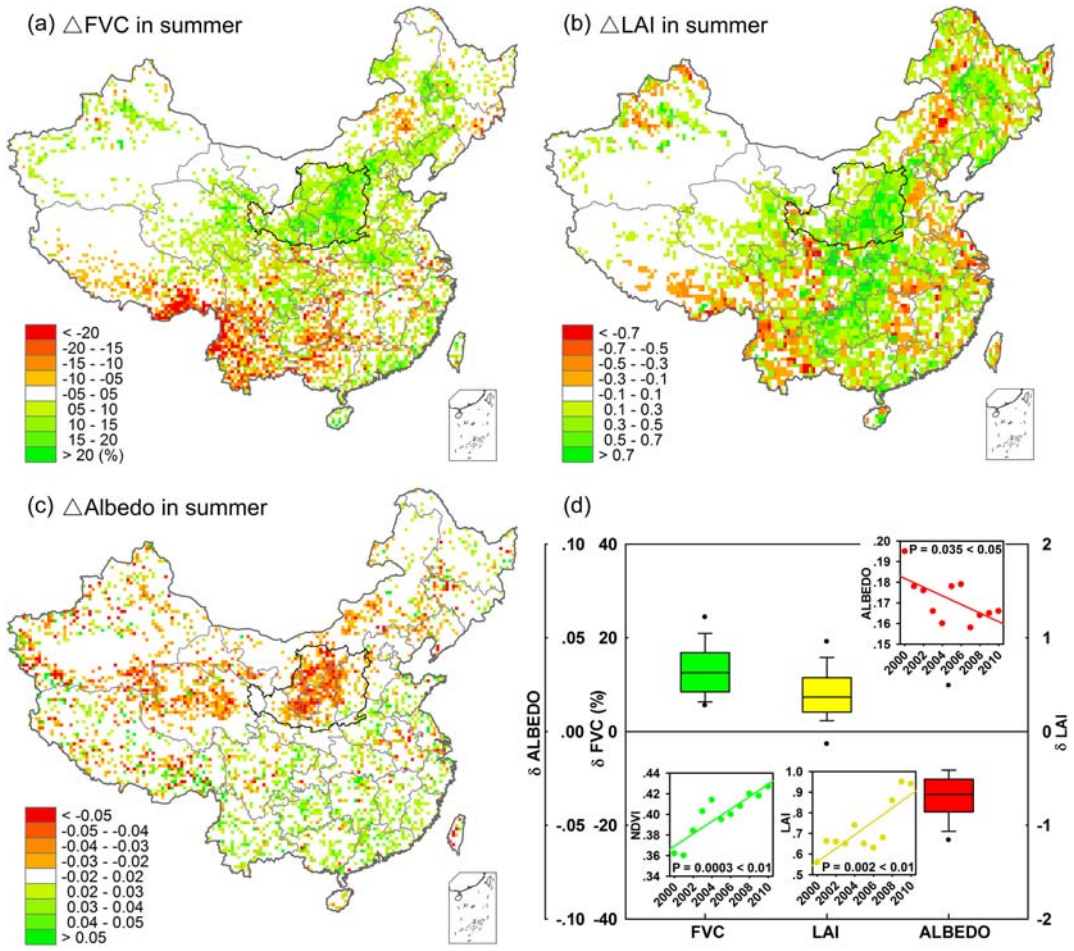

Fig. 4. Spatial pattern of changes in summertime land surface biophysical properties between 2001 and 2010: (a) vegetation fraction (FVC; %), (b) leaf area index (LAI), and (c) surface albedo. Also shown are box and whisker plots of changes in the three parameters between 2001 and 2010 at the Loess Plateau (the region marked with a black solid contour; d). The insets in (d) indicate trends of interannual variations in summertime NDVI, LAI, and surface albedo. Across the Loess Plateau, these trends are statistically significant at the 0.01 level for NDVI and LAI and at the 0.05 level for surface albedo.

increases in surface albedo were estimated in Yunnan province (the southwest of the country, also see Fig. 5).

3.3. Impacts of landscape changes on 2-m air temperature

Here we use ensemble differences in appropriate climate metrics between LS2001 and LS2010 (LS2010 – LS2001) to estimate impacts of landscape changes on summer climate over China. We show that modification of land surface conditions exerted a strong influence on 2-m air temperature across the country (Fig. 5a). In summer, widespread cooling effects were simulated in northern China, with local reduction in 2-m air temperature up to 1.0 °C. Meanwhile, broad warming effects were found in the Tibetan Plateau, the southwest, as well as portions of the North China Plain, with the magnitude of warming generally <0.8 °C. Moreover, our modeling work identified three hotspots of temperature changes: the Northeast, the Loess Plateau, and Yunnan province (Figs. 5b–d).

The Northeast underwent widespread decreases in summer temperature of 0.5 °C on average, with local maximum cooling of 1 °C. Similarly, extensive cooling effects, ranging between 0.6 and 1.0 °C, appeared in the Loess Plateau, with local peak cooling approaching 1.5 °C. However, patchy increases in 2-m air temperature, on the order of 0.2–0.4 °C, were simulated at the southwest of the region. In contrast, considerable warming effects were found in Yunnan province, especially its northern portions, while slight scattered cooling occurred in its southern part. On average, 2-m air temperature decreased by 0.3–0.6 °C in the Northeast and 0.3–0.8 °C in the Loess Plateau, while increasing 0.3–0.5 °C in Yunnan province (see box and whisker plots accompanying Fig. 5b–d). In addition, scattered hotspots occurred in the urbanized areas presented in Fig. 3c, where near-surface warming reached 2 °C.

To validate temperature differences simulated by the WRF model, we further used the OMR approach to calculate landscape modification-induced temperature changes in summer based on a time series of 13 years (from 1999 to 2011) at meteorological stations in the aforementioned three hotspots. The simulation results generally agreed well with the OMR results in terms of both the magnitude and broad spatial pattern, which also indicated considerable cooling effects in the farm belt of the Northeast and the Loess Plateau, as well as non-negligible warming effects in Yunnan province (Fig. 5e–g). The localized discrepancy between the OMR and simulation results in Yunnan may be ascribed partly to the relatively high elevation and complex topography of the region, which usually reduces the accuracy of the OMR approach when applied in mountainous areas. In addition, both the model simulation and OMR analysis exhibited a similar magnitude of warming at the southwest of the Loess Plateau, where cultivated and overgrazed lands were turned into shrublands (see Fig. 3). The strong spatial and quantitative agreement between WRF-simulated 2-m air temperature and the OMR analysis demonstrates the significance of landscape forcing in modulating summertime thermal conditions for China.

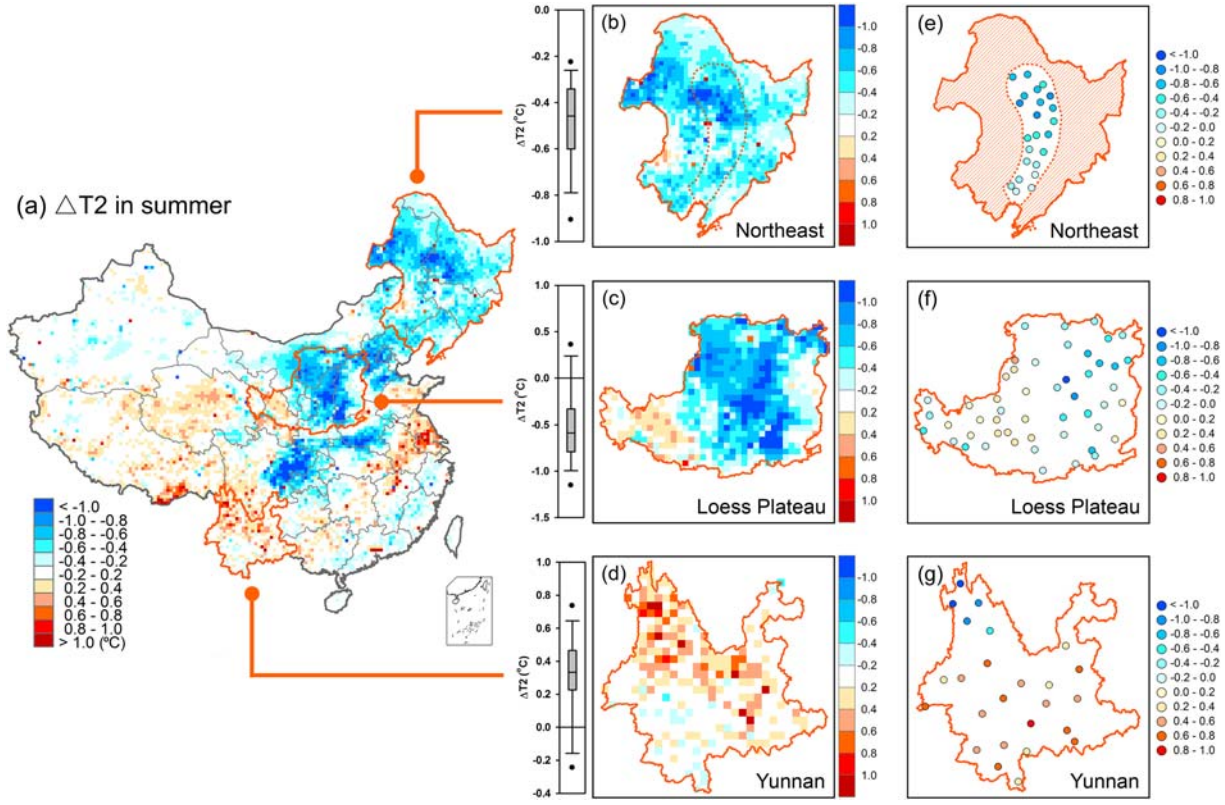

Fig. 5. Spatial pattern of simulated differences (LS2010 – LS2001) in summertime 2-m air temperature (unit: °C) in China (a), the Northeast (b), the Loess Plateau (c), and Yunnan (d). The box and whisker plots of simulated temperature differences for each subregion accompany (b) – (d). Also shown are decadal trends of summertime 2-m air temperature (unit: °C/decade) during the period of 1999 to 2011 at meteorological stations in the farm belt of the Northeast (e), the Loess Plateau (f), and Yunnan (g) as revealed by the observation minus reanalysis (OMR) method.

3.4. Impacts of landscape changes on surface energy budget

The spatial pattern of changes in surface net radiation and albedo exhibited considerable similarity (Fig. 6a). In areas where albedo decreased, the net radiation increased accordingly, and vice versa. Variations in surface radiation flux further resulted in changes in surface energy budget that drove the alterations to 2-m air temperature presented earlier (Figs. 6b–c). In summer, changes in sensible and latent heat fluxes were evident, particularly for regions with substantial modification of vegetation fraction and LAI. Generally, sensible heat flux decreased while latent heat flux increased in regions that experienced near-surface cooling, and vice versa. For example, decreases in sensible heat flux of about 15 W/m^2 and increases in latent heat flux of about 25 W/m^2 were simulated in most portions of the Loess Plateau. Opposite changes, however, were found at the southwest part of the region, where sensible heat flux increased while latent heat flux decreased by 15 W/m^2 on average, with patchy increases in sensible heat flux reaching 30 W/m^2 and patchy reduction in latent heat flux up to 35 W/m^2.

3.5. Impacts of landscape changes on 2-m moisture and heat content

We further examined changes in 2-m water vapor mixing ratio to assess the impacts of landscape changes on low-level atmospheric moisture content over China (Fig. 7a). The region displaying the largest increases in 2-m water vapor mixing ratio (0.4–0.8 g/kg) was located in and around the Loess Plateau. Changes of similar order of magnitude, but of opposite sign (i.e., drying rather than moistening) were found in the northeastern and southeastern parts of China. In contrast with the surroundings, the southwest portions of the Loess Plateau had decreased levels of moisture, where 2-m water vapor ratio was reduced by 0.2 g/kg on average.

These concurrent alterations to 2-m moisture content, in conjunction with changes in 2-m air temperature, can further enhance or weaken near-surface moist enthalpy (i.e., heat content; Fig. 7b), as proposed by Pielke et al. (2004). For instance, although 2-m air temperature was reduced substantially in the Loess Plateau, near-surface heat content underwent minimal changes because of increased specific humidity. In contrast, concurrent decreases in 2-m air temperature and moisture content led to considerable decreases in near-surface heat content in the Northeast. Generally, moist enthalpy increased in western China while decreasing over eastern China.

3.6. Impacts of landscape changes on precipitation

The ensemble differences in summer precipitation illustrate that different landscape patterns affected the hydrometeorological conditions in China. In summer, precipitation in the southern portions of China and the lower reaches of the Yangtze River was reduced substantially, both in excess of 3.6 mm/day (Fig. 8a). By contrast, enhanced precipitation of 1.8 mm/day on average was found in the southwest and southeast parts of the nation. Although precipitation changes were greater in the south than they were in the north in terms of absolute amounts, an assessment of the percentage changes (i.e., (LS2010 – LS2001)/LS2001) indicated the opposing effect (Fig. 8b). This was especially true for arid and semiarid regions such as the Loess Plateau and the Northeast, where the percentage changes in precipitation approached 90% and 50%, respectively. Hence, we focus on the regions that exhibit the greatest percentage changes in precipitation.

To be specific, summer precipitation decreased in the Northeast (Fig. 8c), with patchy reduction generally <1.8 mm/day, while

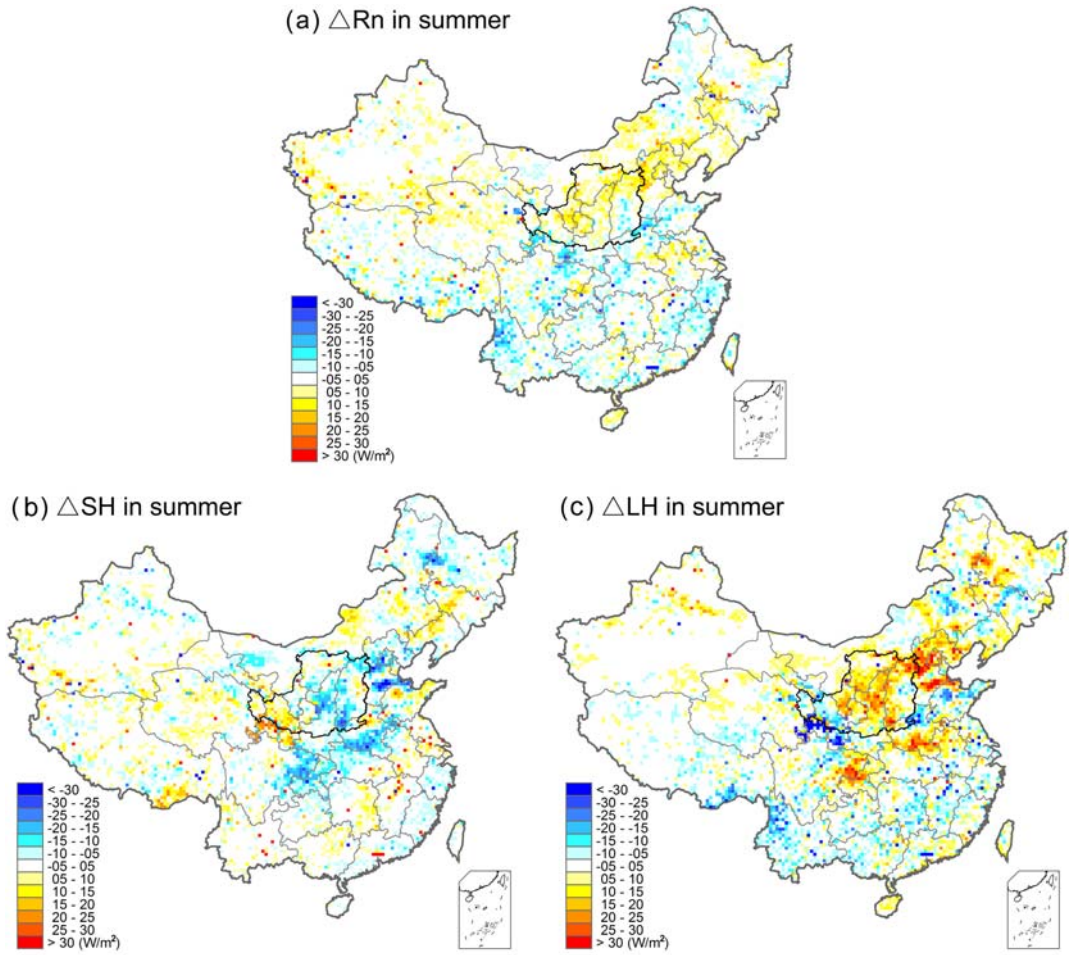

Fig. 6. Spatial pattern of simulated differences (LS2010 – LS2001) in summertime surface net radiation flux (a; Rn), sensible heat flux (b; SH), and latent heat flux (c; LH). Unit: W/m^2.

increasing in the Loess Plateau (Fig. 8d), with this amplification up to 2.4 mm/day in its northern part. The decadal trends of summer precipitation revealed by observing stations in the farm belt of the Northeast also illustrated non-negligible drying effects for the period of 2000 to 2010 (Fig. 8e). Likewise, upward trends of precipitation were found in the northern and southernmost parts of the Loess Plateau, whereas an opposite trend was detected along its eastern border (Fig. 8f). It should be noted that the observed records also exhibited a drying tendency in the southwest of the Loess Plateau.

To examine effects on extreme precipitation, we calculated frequency histograms of simulated summer precipitation to assess the impacts of landscape changes on the distribution of precipitation intensity over China (Fig. 9a). On averwage, landscape changes between 2001 and 2010 tended to homogenize the distribution pattern of precipitation,

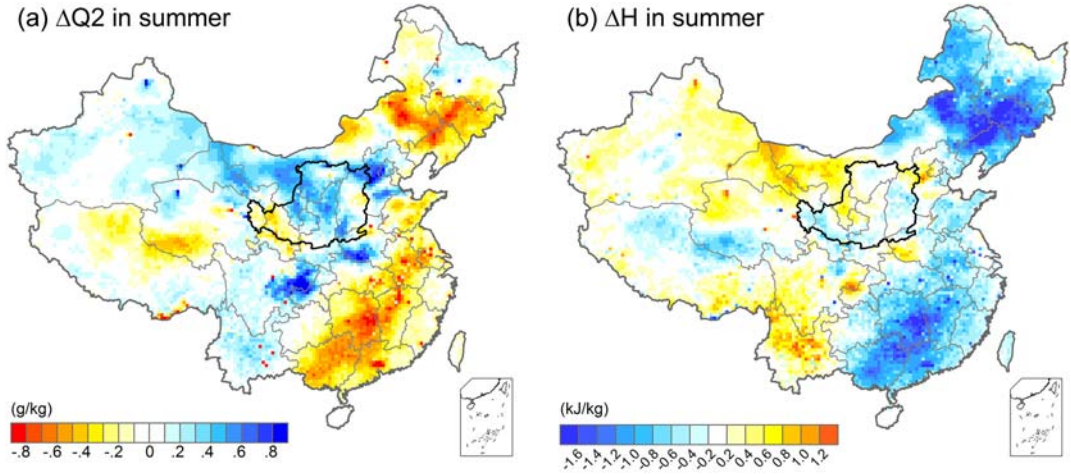

Fig. 7. Spatial pattern of simulated differences (LS2010 – LS2001) in summertime 2-m water vapor mixing ratio (a; Q2) and moist enthalpy (b; H). Unit: g/kg and kJ/kg. The near-surface moist enthalpy (i.e., heat content) is expressed as $H = C_pT + L_vq$, where C_p is the specific heat of air at constant pressure, T the air temperature, L_v the latent heat of vaporization, and q the specific humidity.

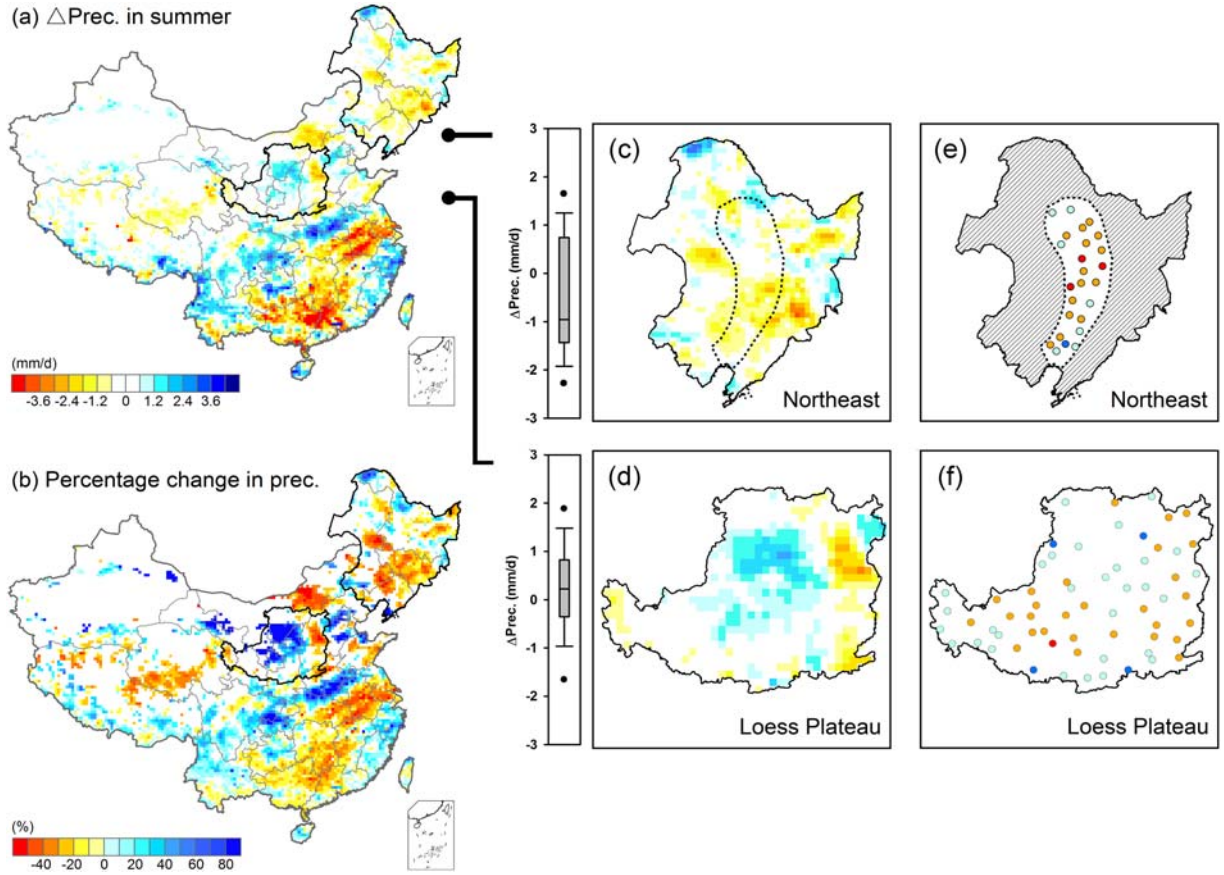

Fig. 8. Spatial pattern of simulated differences (a LS2010 – LS2001; mm/day) and percentage changes (b (LS2010 – LS2001)/LS2001; %) in summer precipitation over China, and spatial pattern as well as box-whisker plots of simulated differences in summer precipitation over the Northeast (c) and the Loess Plateau (d). The decadal trends of summer precipitation on a time series of 13 years (from 1999 to 2011) at observing stations in the farm belt of the Northeast and the Loess Plateau are shown in (e) and (f). Note that ● represents significant increase in precipitation ($p < 0.1$), ○ insignificant increase, ● significant decrease ($p < 0.1$), and ● insignificant decrease.

via the inhibition of low (0–600 mm) and high precipitation (1500–2000 mm), while raising moderate accumulation of precipitation (600–1500 mm). On the regional scale, modification of the intensity of accumulated precipitation exhibited a similar pattern (Figs. 9b–c). For the Loess Plateau, extreme precipitation, especially extreme low (<150 mm), was reduced considerably, while precipitation intensity in between such extreme values (150–570 mm) was raised. Similarly, only the amount of precipitation falling into 350–500 mm increased

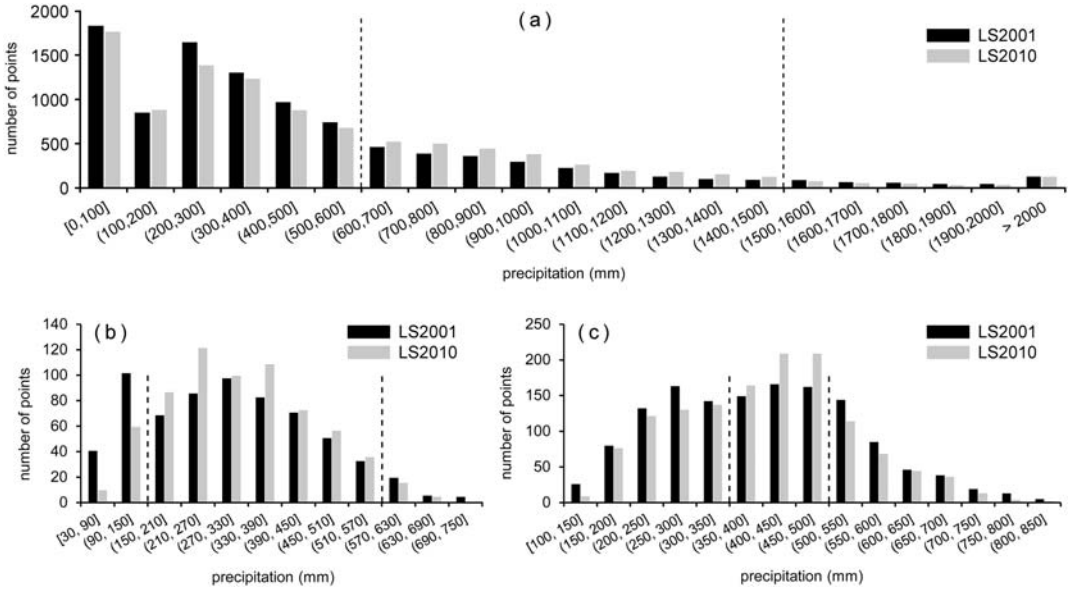

Fig. 9. Frequency histograms of simulated summertime accumulated precipitation distribution (unit: mm), averaged across all three realizations, from LS2001 (black bar) and LS2010 (grey bar) over China (a), the Loess Plateau (b), and the Northeast (c).

over the Northeast, while the relatively low and high precipitation underwent decreased amounts.

4. Discussion

4.1. Landscape changes in China from 2001 to 2010

Our study indicates that there were considerable changes in vegetation fraction (e.g., >20%), leaf area index (e.g., >0.5), and surface albedo (e.g., >0.05) across China between 2001 and 2010. Compared with prior research reporting a climate change-induced increase in NDVI of 0.0007 yr^{-1} from 1982 to 2010 (Peng et al., 2011), changes in land surface properties in our study is several orders of magnitude higher than the values reported previously, suggesting additional factors responsible for the changes in vegetation characteristics between 2001 and 2010. Indeed, a number of recent studies have documented dramatic landscape changes across much of China, especially in the Loess Plateau, the Northeast, and Yunnan, mainly because of changes in national land use policies (Liu et al., 2014; Wu et al., 2015; Shi et al., 2017). For example, since the beginning of the 21st century, Yunnan has been experiencing deforestation, and the situation has become progressively worse during times of severe drought (Yu et al., 2013). Meanwhile, the Chinese government launched the Grain to Green Program so as to restore degraded ecosystems by returning cultivated lands to woodlands as well as overgrazed lands to natural grasslands (Peng et al., 2014). A number of areas in the Loess Plateau and northern China have become greener and more productive since then because of government-supported ecological restoration programs (Xiao, 2014; Feng et al., 2016). However, the mandatory conversion of croplands to ecological restoration areas led to tradeoffs between food supply and demand, especially when urbanization encroached upon sizeable arable lands nationwide (Cao et al., 2016). To alleviate the conflict at the national level, agricultural lands in the fertile Northeast were expanded and intensified (Liu et al., 2014), resulting in increased vegetation fraction and LAI throughout the farmland belt. These landscape modifications, in turn, played an important role in the nation's climatic change and provided the motivation for our regional climate modeling simulations.

4.2. Impacts of landscape changes on summer climate

Compared with prior studies that focused only on the effects of LCC (e.g., Hu et al., 2015; Wang et al., 2013; Wang et al., 2015), our simulation results show that changes in 2-m air temperature were spatially consistent with observations. For instance, previous research investigating the climate response to LCC in China by utilizing 2001 and 2008 land cover conditions found that the most evident increases in summer temperature (about 0.35 °C) appeared in the Loess Plateau, while few changes were found in the southwestern and northeastern parts of the country (Wang et al., 2013). The main reason for these discrepancies was that the amount and spatial heterogeneity of changes in land surface biophysical properties that arise from LMC were neglected and thus led to incorrect surface-absorbed solar energy and the partitioning of available energy into sensible and latent heat fluxes. For our study, however, modification of vegetation characteristics largely determined 2-m air temperature differences via alteration of surface energy budget.

Although our simulations were performed on a model domain discretized with 30-km grid spacing, the magnitude and spatial pattern of summertime 2-m air temperature differences were well simulated. This was partly due to the scale invariant characteristic of satellite-derived vegetation fraction and LAI (Zheng and Moskal, 2009). However, it does not mean that the scale effect can be neglected when employing satellite-derived landscape data to drive climate models. In this work, changes in surface albedo were generally modest in summer. But for regions or seasons with extensive modification of surface albedo or for simulations with incorporation of other land surface biophysical properties, the scale-dependent characteristic of remotely sensed data requires further consideration to accurately assess the impacts of landscape changes on regional climate (Liu et al., 2008). In addition, while our study focused on mean summertime conditions to better distinguish the signal of landscape change-induced forcing, future research should also address different background meteorology.

Regional precipitation changes is not only affected by evapotranspiration but also large-scale dynamics and ascertaining the contribution of landscape change-induced forcing to total observed precipitation is not trivial (Douglas et al., 2009; Degu et al., 2011; Gero et al., 2006; Lei et al., 2008; Nair et al., 2011; Woldemichael et al., 2012). The general consistency of simulated precipitation differences to observed records can at least demonstrate that human activities play a pivotal role in the hydrometeorological behavior of the highlighted regions. Prior research using station-based observations found similar trends of precipitation changes presented in this work, especially for the northeastern portions of China and the Loess Plateau (e.g., Liang et al., 2011; Zhai et al., 2015). Although the amount of precipitation changes revealed by both the simulations and observations was relatively small in the two subregions, the percentage change in precipitation was comparatively large. This suggests that one-unit change in precipitation has greater significance for people residing in arid and semiarid areas.

4.3. Implications for climate change mitigation and adaptation

Our study provides valuable information for landscape management and policy making in terms of climate change mitigation and adaptation. Although revegetation in the Loess Plateau gave rise to increased biomass and thus extensive summer cooling, an exception existed at the southwest of the region, where cultivated fields and overgrazed lands have been converted to shrublands since the implementation of the Grain to Green Program. Consequently, 2-m air temperatures increased in summer owing to decreased latent heat flux but increased sensible heat flux. In addition, minimal changes in summer precipitation were simulated there, while the observations revealed a downward trend. This was because the replacement of grasslands by woody plants in water-limited areas restricted the growth of woody plants and thus the evapotranspiration of vegetation through which regional climate was regulated. Therefore, afforestation in arid and semiarid areas should proceed with caution (Feng et al., 2016).

Furthermore, as the highest pole in the world, the Tibetan Plateau exerts a strong influence on regional and global climate as well as water supply. Both observations and reanalysis data have revealed a sustained warming trend in the Tibetan Plateau that was higher than the estimated global average since the late 1980s (Kang et al., 2010). The physical drivers of this amplification were partially attributed to land surface modification: grassland degradation, urbanization, deforestation, and desertification (Kang et al., 2010). Based on the OMR analysis, a non-negligible signal of landscape change-induced summer warming was found in the Tibetan Plateau (You et al., 2013), which was consistent with our simulation results. Notably, as the source of the three longest rivers in China (i.e., the Yellow River, the Yangtze River, and the Lantsang River), glacier ablation in the Tibetan Plateau as a result of continuous warming will have severe environmental consequences far beyond climate change. Hence, conservation of its extensive fragile ecosystems is essential not only for China, but also for Southeast Asia.

5. Conclusions

Our study establishes the first comprehensive assessment of the impacts of landscape changes on summer climate over China during 2001–2010, using a coupled process-based land-atmospheric model. The distinct climate change hotspots across the country are revealed through incorporation of real-time and high-quality satellite-derived land surface biophysical properties (i.e., vegetation fraction, leaf area index, and surface albedo) to represent land management change, in

contrast to prior studies that focused only on the effects of land cover change (e.g., Hu et al., 2015; Wang et al., 2013; Wang et al., 2015). By explicitly considering the amount and spatial heterogeneity of alterations to biophysical properties that arise from changes in both land cover and land management, our study provides robust estimates of the magnitude and spatial pattern of climate impacts induced by landscape changes in China, which can be useful for developing regional- and national-level climate mitigation and adaptation strategies.

Acknowledgements

Our study is financially supported by the National Basic Research Program of China (grant number: 2014CB954301), the National Natural Science Foundation of China (grant number: 41571170), and the Science Fund for Creative Research Groups (grant number: 41321001). Matei Georgescu is supported by the National Science Foundation Sustainability Research Network (SRN): Urban Water Innovation Network (U-WIN; grant number: 1444758). We are grateful to the Institute of Geographic Sciences and Natural Resources Research, Chinese Academy of Sciences for allocating supercomputer resources. We also thank Professor Crystal Schaaf's Lab at University of Massachusetts-Boston for providing the gap-filled albedo product and Xiaoyuan Li for gathering the meteorological data.

Competing interests

The authors declare no competing interests.

References

Betts, R.A., Falloon, P.D., Goldewijk, K.K., Ramankutty, N., 2007. Biogeophysical effects of land use on climate: model simulations of radiative forcing and large-scale temperature change. Agric. For. Meteorol. 142, 216–233.
Cao, Q., Yu, D., Georgescu, M., Han, Z., Wu, J., 2015. Impacts of land use and land cover change on regional climate: a case study in the agro-pastoral transitional zone of China. Environ. Res. Lett. 10, 124025.
Cao, Q., Yu, D., Georgescu, M., Wu, J., 2016. Impacts of urbanization on summer climate in China: an assessment with coupled land-atmospheric modeling. J. Geophys. Res. Atmos. 121, 10,505–10,521.
Chen, F., Dudhia, J., 2001. Coupling an advanced land surface-hydrology model with the Penn State-NCAR MM5 modeling system. Part I: model implementation and sensitivity. Mon. Weather Rev. 129, 569–585.
Davin, E.L., de Noblet-Ducoudré, N., Friedlingstein, P., 2007. Impact of land cover change on surface climate: relevance of the radiative forcing concept. Geophys. Res. Lett. 34, L13702.
Degu, A.M., Hossain, F., Niyogi, D., Pielke, R., Shepherd, J.M., Voisin, N., Chronis, T., 2011. The influence of large dams on surrounding climate and precipitation patterns. Geophys. Res. Lett. 38, L04405.
Douglas, E.M., Beltrán-Przekurat, A., Niyogi, D., Pielke, R.A., Vörösmarty, C.J., 2009. The impact of agricultural intensification and irrigation on land-atmosphere interactions and Indian monsoon precipitation-A mesoscale modeling perspective. Glob. Planet. Chang. 67, 117–128.
Ek, M.B., Mitchell, K.E., Lin, Y., Rogers, E., Grunmann, P., Koren, V., Gayno, G., Tarpley, J.D., 2003. Implementation of Noah land surface model advances in the National Centers for Environmental Prediction operational mesoscale Eta model. J. Geophys. Res. Atmos. 108, D228851.
Feddema, J.J., Oleson, K.W., Bonan, G.B., Mearns, L.O., Buja, L.E., Meehl, G.A., Washington, W.M., 2005. The importance of land-cover change in simulating future climates. Science 310, 1674–1678.
Feng, X., Fu, B., Piao, S., Wang, S., Ciais, P., Zeng, Z., Lü, Y., Zeng, Y., Li, Y., Jiang, X., Wu, B., 2016. Revegetation in China's Loess Plateau is approaching sustainable water resource limits. Nat. Clim. Chang. 6, 1019–1022.
Foley, J.A., DeFries, R., Asner, G.P., Barford, C., Bonan, G., Carpenter, S.R., Chapin, F.S., Coe, M.T., Daily, G.C., Gibbs, H.K., Helkowski, J.H., Holloway, T., Howard, E.A., Kucharik, C.J., Monfreda, C., Patz, J.A., Prentice, I.C., Ramankutty, N., Snyder, P.K., 2005. Global consequences of land use. Science 309, 570–574.
Fu, C., 2003. Potential impacts of human-induced land cover change on East Asia monsoon. Glob. Planet. Chang. 37, 219–229.
Gao, G., Fu, B., Wang, S., Liang, W., Jiang, X., 2016. Determining the hydrological responses to climate variability and land use/cover change in the Loess Plateau with the Budyko framework. Sci. Total Environ. 557, 331–342.
Georgescu, M., Lobell, D.B., Field, C.B., 2009. Potential impact of US biofuels on regional climate. Geophys. Res. Lett. 36, L21806.
Georgescu, M., Moustaoui, M., Mahalov, A., Dudhia, J., 2013. Summer-time climate impacts of projected megapolitan expansion in Arizona. Nat. Clim. Chang. 3, 37–41.
Gero, A.F., Pitman, A.J., Narisma, G.T., Jacobson, C., Pielke, R.A., 2006. The impact of land cover change on storms in the Sydney Basin, Australia. Glob. Planet. Chang. 54, 57–78.
Gutman, G., Ignatov, A., 1998. The derivation of the green vegetation fraction from NOAA/AVHRR data for use in numerical weather prediction models. Int. J. Remote Sens. 19, 1533–1543.
Hu, Y., Zhang, X., Mao, R., Gong, D., Liu, H., Yang, J., 2015. Modeled responses of summer climate to realistic land use/cover changes from the 1980s to the 2000s over eastern China. J. Geophys. Res. Atmos. 120, 167–179.
Kabat, P., 2004. Vegetation, Water, Humans and the Climate: A New Perspective on an Internactive System. Springer Science & Business Media, Berlin.
Kalnay, E., Cai, M., 2003. Impact of urbanization and land-use change on climate. Nature 423, 528–531.
Kanamitsu, M., Ebisuzaki, W., Woollen, J., Shi-Keng, Y., 2002. NCEP-DOE AMIP-II reanalysis (R-2). Bull. Am. Meteorol. Soc. 83, 1631–1643.
Kang, S., Xu, Y., You, Q., Flügel, W.A., Pepin, N., Yao, T., 2010. Review of climate and cryospheric change in the Tibetan Plateau. Environ. Res. Lett. 5, 015101.
Lei, M., Niyogi, D., Kishtawal, C., Pielke, R.A., Beltrán-Przekurat, A., Nobis, T.E., Vaidya, S.S., 2008. Effect of explicit urban land surface representation on the simulation of the 26 July 2005 heavy rain event over Mumbai, India. Atmos. Chem. Phys. 8, 5975–5995.
Li, Z., Yan, Z., 2009. Homogenized daily mean/maximum/minimum temperature series for China from 1960-2008. Atmos. Ocean. Sci. Lett. 2, 237–243.
Li, J., Zeng, Q., 2005. A new monsoon index, its interannual variability and relation with monsoon precipitation. Climatic. Environ. Res. 10, 351–365.
Liang, X., Xu, M., Gao, W., Kunkel, K., Slusser, J., Dai, Y., Min, Q., Houser, P.R., Rodell, M., Schaaf, C.B., Gao, F., 2005. Development of land surface albedo parameterization based on moderate resolution imaging spectroradiometer (MODIS) data. J. Geophys. Res. Atmos. 110, D11107.
Liang, L., Li, L., Liu, Q., 2011. Precipitation variability in Northeast China from 1961 to 2008. J. Hydrol. 404, 67–76.
Liu, H., Tu, G., Dong, W., 2008. Three-year changes of surface albedo of degraded grassland and cropland surfaces in a semiarid area. Chin. Sci. Bull. 53, 1246–1254.
Liu, J., Kuang, W., Zhang, Z., Xu, X., Qin, Y., Ning, J., Zhou, W., Zhang, S., Li, R., Yan, C., Wu, S., Shi, X., Jiang, N., Yu, D., Pan, X., Chi, W., 2014. Spatiotemporal characteristics, patterns and causes of land use changes in China since the late 1980s. J. Geogr. Sci. 69, 3–14.
Long, C., Gaustad, K., 2004. The Shortwave (SW) Clear-Sky Detection and Fitting Algorithm: Algorithm Operational Details and Explanations. US, Pacific Northwest National Laboratory.
Luyssaert, S., Jammet, M., Stoy, P.C., Estel, S., Pongratz, J., Ceschia, E., Churkina, G., Don, A., Erb, K., Ferlicoq, M., Gielen, B., Grünwald, T., Houghton, R.A., Klumpp, K., Knohl, A., Kolb, T., Kuemmerle, T., Laurila, T., Lohila, A., Loustau, D., McGrath, M.J., Meyfroidt, P., Moors, E.J., Naudts, K., Novick, K., Otto, J., Pilegaard, K., Pio, C.A., Rambal, S., Rebmann, C., Ryder, J., Suyker, A.E., Varlagin, A., Wattenbach, M., Dolman, A.J., 2014. Land management and land-cover change have impacts of similar magnitude on surface temperature. Nat. Clim. Chang. 4, 389–393.
Mahmood, R., Pielke, R.A., Hubbard, K.G., Niyogi, D., Dirmeyer, P.A., McAlpine, C., Carleton, A.M., Hale, R., Gameda, S., Beltran-Przekurat, A., Baker, B., McNider, R., Legates, D.R., Shepherd, M., Du, J., Blanken, P.D., Frauenfeld, O.W., Nair, U.S., Fall, S., 2014. Land cover changes and their biogeophysical effects on climate. Int. J. Climatol. 34, 929–953.
Mahmood, R., Pielke, R.A., Loveland, T.R., McAlpine, C.A., 2016. Climate relevant land use and land cover change policies. Bull. Am. Meteorol. Soc. 97, 195–202.
Marland, G., Pielke, R.A., Apps, M., Avissar, R., Betts, R.A., Davis, K.J., Frumhoff, P.C., Jackson, S.T., Joyce, L.A., Kauppi, P., Katzenberger, J., MacDicken, K.G., Neilson, R.P., Niles, J.O., Niyogi, D., Norby, R.J., Pena, N., Sampson, N., Xue, Y., 2003. The climatic impacts of land surface change and carbon management, and the implications for climate-change mitigation policy. Clim. Pol. 3, 149–157.
Moody, E.G., King, M.D., Schaaf, C.B., Platnick, S., 2008. MODIS-derived spatially complete surface albedo products: spatial and temporal pixel distribution and zonal averages. J. Appl. Meteorol. Climatol. 47, 2879–2894.
Nair, U.S., Wu, Y., Kala, J., Lyons, T.J., Pielke, R.A., Hacker, J.M., 2011. The role of land use change on the development and evolution of the west coast trough, convective clouds, and precipitation in southwest Australia. J. Geophys. Res. Atmos. 116, D07103.
National Research Council, 2005. Radiative Forcing of Climate Change: Expanding the Concept and Addressing Uncertainties. National Academies Press, Washington DC.
de Noblet-Ducoudré, N., Boisier, J.P., Pitman, A., Bonan, G.B., Brovkin, V., Cruz, F., Delire, C., Gayler, V., van den Hurk, B.J.J.M., Lawrence, P.J., van der Molen, M.K., Müller, C., Reick, C.H., Strengers, B.J., Voldoire, A., 2012. Determining robust impacts of land-use-induced land cover changes on surface climate over North America and Eurasia: results from the first set of LUCID experiments. J. Clim. 25, 3261–3281.
Peng, S., Chen, A., Xu, L., Cao, C., Fang, J., Myneni, R.B., Pinzon, J.E., Tucker, C.J., Piao, S., 2011. Recent change of vegetation growth trend in China. Environ. Res. Lett. 6, 044027.
Peng, S., Piao, S., Zeng, Z., Ciais, P., Zhou, L., Li, L.Z.X., Myneni, R.B., Yin, Y., Zeng, H., 2014. Afforestation in China cools local land surface temperature. Proc. Natl. Acad. Sci. U. S. A. 111, 2915–2919.
Pielke, R.A., Avissar, R., 1990. Influence of landscape structure on local and regional climate. Landsc. Ecol. 4, 133–155.
Pielke, R.A., Davey, C., Morgan, J., 2004. Assessing "global warming" with surface heat content. Eos. Trans. AGU 85, 210–211.
Pielke, R.A., Pitman, A., Niyogi, D., Mahmood, R., McAlpine, C., Hossain, F., Klein Goldewijk, K., Nair, U., Betts, R., Fall, S., Reichstein, M., Kabat, P., de Noblet, N., 2011. Land use/land cover changes and climate: modeling analysis and observational evidence. WIRES. Clim. Chang. 2, 828–850.
Pielke, R.A., Mahmood, R., McAlpine, C., 2016. Land's complex role in climate change. Phys. Today 69, 40–46.
Sellers, P.J., Tucker, C.J., Collatz, G.J., Los, S.O., Justice, C.O., Dazlich, D.A., Randall, D.A., 1996. A revised land surface parameterization (SiB2) for atmospheric GCMs. Part II: the generation of global fields of terrestrial biophysical parameters from satellite data. J. Clim. 9, 706–737.

Shi, P., Bai, X., Kong, F., et al., 2017. Urbanization and air quality as major drivers of altered spatiotemporal patterns of heavy rainfall in China. Landsc. Ecol. 32, 1723–1738.
Skamarock, W.C., Klemp, J.B., 2008. A time-split nonhydrostatic atmospheric model for weather research and forecasting applications. J. Comput. Phys. 227, 3465–3485.
Vitousek, P.M., Mooney, H.A., Lubchenco, J., Melillo, J.M., 1997. Human domination of Earth's ecosystems. Science 277, 494–499.
Wang, Y., Feng, J., Gao, H., 2013. Numerical simulation of the impact of land cover change on regional climate in China. Theor. Appl. Climatol. 115, 141–152.
Wang, M., Xiong, Z., Yan, X., 2015. Modeling the climatic effects of the land use/cover change in eastern China. Phys. Chem. Earth 87–88, 97–107.
Weaver, C.P., Avissar, R., 2001. Atmospheric disturbances caused by human modification of the landscape. Bull. Am. Meteorol. Soc. 82, 269–281.
Woldemichael, A.T., Hossain, F., Pielke, R., Beltrán-Przekurat, A., 2012. Understanding the impact of dam-triggered land use/land cover change on the modification of extreme precipitation. Water Resour. Res. 48, W09547.
Wu, F., Zhan, J., Yan, H., Shi, C., Huang, J., 2013. Land cover mapping based on multisource spatial data mining approach for climate simulation: a case study in the farming-pastoral ecotone of North China. Adv. Meteorol. 2013, 520803.
Wu, J., Xiang, W., Zhao, J., 2014. Urban ecology in China: historical developments and future directions. Landsc. Urban Plan. 125, 222–233.
Wu, J., Zhang, Q., Li, A., Liang, C., 2015. Historical landscape dynamics of Inner Mongolia: patterns, drivers, and impacts. Landsc. Ecol. 30, 1579–1598.
Xiao, J., 2014. Satellite evidence for significant biophysical consequences of the "grain for green" program on the Loess Plateau in China. J. Geophys. Res. Biogeosci. 119, 2261–2275.
Xiao, Z., Liang, S., Wang, J., Chen, P., Yin, X., Zhang, L., Song, J., 2014. Use of general regression neural networks for generating the GLASS leaf area index product from time-series MODIS surface reflectance. IEEE T. Geosci. Remote 52, 209–223.
Xu, Y., Gao, X., Shen, Y., Xu, C., Shi, Y., Giorgi, F., 2009. A daily temperature dataset over China and its application in validating a RCM simulation. Adv. Atmos. Sci. 26, 763–772.
Xu, Z., Mahmood, R., Yang, Z., Fu, C., Su, H., 2015. Investigating diurnal and seasonal climatic response to land use and land cover change over monsoon Asia with the community earth system model (CESM). J. Geophys. Res. Atmos. 120, 1137–1152.
You, Q., Fraedrich, K., Ren, G., Pepin, N., Kang, S., 2013. Variability of temperature in the Tibetan Plateau based on homogenized surface stations and reanalysis data. Int. J. Climatol. 33, 1337–1347.
Yu, W., Shao, M., Ren, M., Zhou, H., Jiang, Z., Li, D., 2013. Analysis on spatial and temporal characteristics drought of Yunnan Province. Acta Ecol. Sin. 33, 317–324.
Zhai, J., Liu, R., Liu, J., Huang, L., Qin, Y., 2015. Human-induced landcover changes drive a diminution of land surface albedo in the Loess Plateau (China). Remote Sens. 7, 2926–2941.
Zheng, G., Moskal, L.M., 2009. Retrieving leaf area index (LAI) using remote sensing: theories, methods and sensors. Sensors 9, 2719–2745.